

Patient-Specific Dosimetry of Pretargeted Radioimmunotherapy Using CC49 Fusion Protein in Patients with Gastrointestinal Malignancies

Sui Shen, PhD¹; Andres Forero, MD²; Albert F. LoBuglio, MD²; Hazel Breitz, MD³; M.B. Khazaeli, PhD¹; Darrell R. Fisher, PhD⁴; Wenquan Wang, PhD⁵; and Ruby F. Meredith, MD, PhD¹

¹Department of Radiation Oncology, Comprehensive Cancer Center, University of Alabama at Birmingham, Birmingham, Alabama;

²Department of Medicine, Comprehensive Cancer Center, University of Alabama at Birmingham, Birmingham, Alabama; ³NeoRx Corp., Seattle, Washington; and ⁴Pacific Northwest National Laboratory, Richland, Washington; and ⁵Biostatistics Division, Comprehensive Cancer Center, University of Alabama at Birmingham, Birmingham, Alabama

Pretargeted radioimmunotherapy (RIT) using CC49 fusion protein, comprised of CC49-(scFv)₄ and streptavidin, in conjunction with ⁹⁰Y/¹¹¹In-DOTA-biotin (DOTA = dodecanetetraacetic acid) provides a new opportunity to improve efficacy by increasing the tumor-to-normal tissue dose ratio. To our knowledge, the patient-specific dosimetry of pretargeted ⁹⁰Y/¹¹¹In-DOTA-biotin after CC49 fusion protein in patients has not been reported previously. **Methods:** Nine patients received 3-step pretargeted RIT: (a) 160 mg/m² of CC49 fusion protein, (b) synthetic clearing agent (sCA) at 48 or 72 h later, and (c) ⁹⁰Y/¹¹¹In-DOTA-biotin 24 h after the sCA administration. Sequential whole-body ¹¹¹In images were acquired immediately and at 2–144 h after injection of ⁹⁰Y/¹¹¹In-DOTA-biotin. Geometric-mean quantification with background and attenuation correction was used for liver and lung dosimetry. Effective point source quantification was used for spleen, kidneys, and tumors. Organ and tumor ⁹⁰Y doses were calculated based on ¹¹¹In imaging data and the MIRD formalism using patient-specific organ masses determined from CT images. Patient-specific marrow doses were determined based on radioactivity concentration in the blood. **Results:** The ⁹⁰Y/¹¹¹In-DOTA-biotin had a rapid plasma clearance, which was biphasic with <10% residual at 8 h. Organ masses ranged from 1,263 to 3,855 g for liver, 95 to 1,009 g for spleen, and 309 to 578 g for kidneys. The patient-specific mean ⁹⁰Y dose (cGy/37 MBq, or rad/mCi) was 0.53 (0.32–0.78) to whole body, 3.75 (0.63–6.89) to liver, 2.32 (0.58–4.46) to spleen, 7.02 (3.36–11.2) to kidneys, 0.30 (0.09–0.44) to lungs, 0.22 (0.12–0.34) to marrow, and 28.9 (4.18–121.6) to tumors. **Conclusion:** Radiation dose to normal organs from circulating radionuclide is substantially reduced using pretargeted RIT. Tumor-to-normal organ dose ratios were increased about 8- to 11-fold compared with reported patient-specific mean dose to liver, spleen, marrow, and tumors from ⁹⁰Y-CC49.

Key Words: gastrointestinal cancer; dosimetry; pretargeted radioimmunotherapy

J Nucl Med 2005; 46:642–651

Metastatic or recurrent gastrointestinal (GI) cancer is a common cause of morbidity and mortality in the United States. If not cured by surgery, chemotherapy regimens produce, at best, modest effects on survival. Once failure occurs with first-line chemotherapy, further attempts at chemotherapy produce minimal benefits and survival is about 3–9 mo. Radiotherapy has a limited local control, palliative role in a small group of patients. Therefore, innovative therapies are needed for metastatic or recurrent GI cancer.

Radioimmunotherapy (RIT) is one innovative approach that systemically delivers localized radiation through an antibody directed to a tumor-associated antigen. Encouraging results have been obtained in RIT for lymphoma (1–4). However, the effect of RIT on metastatic or recurrent GI cancer has been disappointing. Prior phase I and phase II studies with the CC49 antibody have generally shown localization of radiolabeled antibodies to tumor sites but with insufficient radiation delivery to produce objective tumor regression (5–9). The efficacy of radiolabeled antibodies for GI cancer, in general, has been limited by several factors, including (a) slow accumulation at tumor sites, (b) relatively slow clearance from the blood, and (c) radioresistance of the tumors. Consequently, although tumors receive insufficient radiation for an objective response, the radiation dose to radiosensitive normal organs has already exceeded the maximum tolerable limit.

The pretargeted RIT (Pretarget RIT; NeoRx Corp.) system has been developed to address 2 of these factors (10–16). Because a targeting molecule administered first is not radiolabeled, the pretargeted RIT system does not suffer from prolonged radiation to normal organs due to slow accumulation at tumor sites. Since the radionuclide is delivered later on a small molecule (<1 kDa) that is rapidly excreted through the kidneys, radiation dose to normal organs from circulating radionuclide is substan-

Received Mar. 25, 2004; revision accepted Nov. 17, 2004.

For correspondence or reprints contact: Sui Shen, PhD, Department of Radiation Oncology, University of Alabama at Birmingham, 1824 6th Ave. S., Wallace Tumor Institute Room 124, Birmingham, AL 35294.

E-mail: sshen@uabmc.edu

tially reduced. Thus, tumor-to-normal organ dose ratios are expected to improve by this approach.

We have conducted a phase I trial using pretargeted CC49 fusion protein. The CC49 fusion protein is a genetic fusion of the single-chain variable region (scFv) of the murine antibody that targets TAG-72 and streptavidin (SA). Expression results in spontaneous folding into a tetramer containing 4 scFv of CC49 and the 4 subunits of SA. After pretargeting with CC49 fusion protein and use of synthetic clearing agent (sCA) to clear unbound fusion protein, $^{111}\text{In}/^{90}\text{Y}$ -DOTA-biotin (DOTA = dodecanetetraacetic acid) was injected to deliver ^{90}Y radiation to tumor sites. To our knowledge, this is the first study to determine the tissue distribution of $^{90}\text{Y}/^{111}\text{In}$ -DOTA-biotin after CC49 fusion protein by quantitative imaging and to report its radiation dosimetry for tumors and normal organs.

MATERIALS AND METHODS

Patients

Nine patients with previously treated metastatic colorectal cancer were enrolled in this study. These patients had failed at least 1 and no more than 3 prior therapy regimens. All patients had measurable tumors that were TAG-72 positive (>30% of cells) on immunoperoxidase staining, and patients had a negative antibody response to CC49 fusion protein. The median age was 58 y (range, 53–78 y).

Pretargeting Components

The 3 steps of administering the pretargeting components have been previously described (11,12). The first of 3 steps involves the injection of the CC49 fusion protein that targets TAG-72. After allowing peak CC49-(scFv)₄SA levels to accrete at the tumor, a synthetic biotin galactosamine clearing agent (sCA), is injected to remove unbound CC49-(scFv)₄SA from the circulation. Finally, DOTA-biotin radiolabeled with $^{90}\text{Y}/^{111}\text{In}$ is injected and distributes rapidly throughout the vascular and extravascular space. All components were manufactured, tested, and released by NeoRx Corp. to the University of Alabama at Birmingham. Doses of the components and intervals between them were guided by preclinical studies and prior clinical trials of pretargeted RIT (10–16). All patients received 160 mg/m² of CC49-(scFv)₄SA. The sCA was administered either 48 or 72 h after CC49-(scFv)₄SA at a dose of 45 mg/m². The third component, $^{90}\text{Y}/^{111}\text{In}$ -DOTA-biotin, was then administered 24 h after the sCA at a dose of 0.65 or 1.3 mg/m² (Table 1). All patients received 185 MBq (5 mCi) ^{111}In -labeled DOTA-biotin for imaging and dosimetry purposes, and patients 4–9 also received 370 MBq/m² (10 mCi/m²) of ^{90}Y at the same time.

Quantification of $^{90}\text{Y}/^{111}\text{In}$ in Serum

Blood samples were collected before, at 5, 15, and 30 min, and at 1, 2, 4, 6, 8, 12, 24, 48, and 72 h after the administration of the radiolabeled DOTA-biotin. The ^{90}Y dose to marrow for patients 1–3 was derived from ^{111}In , and ^{111}In activity was measured using a γ -well counter. The ^{90}Y in serum for patients 4–9 was directly measured using liquid scintillation counting. The activities of ^{90}Y - and ^{111}In -DOTA-biotin were corrected for decay of the radioisotope from the time of drug administration to the time of measurement by counting the samples and the standards at the same time. ^{90}Y - and ^{111}In -DOTA-biotin concentration was expressed as percentage injected dose per milliliter (%ID/mL) and analyzed using a biexponential clearance (α and β) model. Patients 4–9 had both ^{90}Y and ^{111}In concentrations measured. To compare the similarity between ^{90}Y and ^{111}In concentrations, mean weighted %ID/mL was computed to average all sample time points:

$$\text{mean weighted}(\% \text{ID/mL}) = \sum_i w_i (\% \text{ID/mL})_i, \quad \text{Eq. 1}$$

where i is i th sample time point, w_i is the weight at i point, and w_i equals $(\% \text{ID/mL})_i / \sum (\% \text{ID/mL})_i$.

Quantitative Imaging

Planar conjugate whole-body images were acquired with a Philips dual-detector γ -camera interfaced to a nuclear medicine computer system (Philips Medical System). The detectors had a 3/4-in.-thick (19 mm) NaI(Tl) crystal. Medium-energy collimators were used to image ^{111}In with energy windows centered at 171 and 245 keV (15% width). Transmission scan images were obtained using a ^{57}Co sheet source containing about 370 MBq (10 mCi). The same medium-energy collimators were used to image ^{57}Co with an energy window centered at 122 keV (15% width).

Phantom Study. To determine attenuation correction factors for the dual-detector γ -camera, 3 plastic bottles containing 50, 150, and 1,570 mL of ^{111}In solution were used to simulate tumor, kidney/spleen, and liver, respectively. Liver was quantified using geometric-mean quantification (17), and an attenuation correction factor was determined by flood transmission scan. Transmission images were acquired with the liver phantom ^{111}In solution placed on solid water blocks of various thickness (2–24 cm). Transmission fractions were determined by comparing counts in the liver phantom region of interest (ROI) with and without solid water blocks. ^{57}Co flood transmission images were also acquired with 2- to 24-cm solid water blocks. The liver phantom ROI defined from the ^{111}In image was transferred to define the ROI for the ^{57}Co images. Transmission fractions of ^{57}Co counts were determined by comparing counts in the ROI with and without solid water blocks. Effec-

TABLE 1
Patient Cohorts in the Trial

Cohort	Patient no.	CC49 fusion protein (mg/m ²)	Interval 1 (h)	sCA (mg/m ²)	Interval 2 (h)	$^{111}\text{In}/^{90}\text{Y}$ -DOTA-biotin
1	1–3	160	72	45	24	^{111}In -DOTA-biotin, 1.3 mg/m ²
2	4–6	160	48	45	24	^{111}In - and ^{90}Y -DOTA-biotin, 1.3 mg/m ²
3	7–9	160	48	45	24	^{111}In - and ^{90}Y -DOTA-biotin, 0.65 mg/m ²

tive linear attenuation coefficients, $\mu^{57\text{Co}}$ and $\mu^{111\text{In}}$, were determined from these transmission fractions.

Since previous studies suggested that geometric-mean quantification was accurate only for a large source that was visible on both conjugate views, attenuation correction factors for kidney, spleen, and tumor were determined by the effective point source method (18). Attenuation correction factors for relatively small sources were determined using 50- and 150-mL ^{111}In sources placed on solid water blocks. Transmission fractions were determined by comparing counts in the source ROI with and without the blocks of various thickness (2–24 cm).

Patient Studies. Planar conjugate views of the whole body were acquired immediately after administration of $^{90}\text{Y}/^{111}\text{In}$ -DOTA-biotin and at 2, 24, 48, and 120 or 144 h. Whole-body images were acquired in a $256 \times 1,024$ word matrix with a scan speed of 8–10 cm/min. Each patient's position on the imaging table and vertical positions of the camera detectors were recorded in the first imaging session and were used throughout the sequential imaging studies for reproducible detector-to-patient positioning. A 20-mL ^{111}In reference source containing 1.9–3.7 MBq (50–100 μCi) was placed on the imaging table at least 10 cm away from the patient's feet. The number of counts from this reference source was used to convert the counts in the tissue ROI to radioactivity in the tissue.

Before processing images, the operator reviewed the medical record, CT report, and CT images with the physicians for organ and tumor ROI determination. Major organs that were visible above body background after clearance of the blood pool were quantified. Although tumors were visible for each patient, tumors were quantified only if they met the following criteria for adequate accuracy: (a) ≥ 1 cm in diameter, (b) tumor-to-background pixel counts ratio of ≥ 1.5 (19), and (c) clear tumor ROI boundary. Some liver tumor masses were diffusely distributed and were excluded from image quantification. If a liver tumor appeared as a single mass (ROI) on γ -camera images but appeared as a group of several adjacent masses within the ROI on CT images, tumor mass was determined by excluding the portion of normal liver within the ROI on CT images.

Counts in ROIs were background corrected to subtract counts contributed from radioactivity in the background volume. Background ROIs were selected in regions of the body that had a thickness equivalent to that of the overlapping background volume for the organ or tumor for background ROI subtraction. Special attention was given to background subtraction for liver tumors because the tumors overlapped normal liver and soft-tissue background volumes. Two background ROIs were determined: one outside the liver and one adjacent to the tumor inside the liver. The thickness of the body background ROI outside the liver, the thickness of the liver ROI next to the tumor, and the thickness of the body soft tissue that overlapped with the tumor ROI and liver ROI were measured from CT for each liver tumor. These measurements were used to adjust the counts contributed from overlapped liver and soft-tissue background volumes.

The geometric-mean quantification was used to determine activities in the liver and lungs. The attenuation correction factor, ACF, was determined by:

$$\text{ACF}_{^{111}\text{In}} = \left(\sqrt{\frac{N_{\text{no pt}}}{N_{\text{pt}}}} \right)^{(\mu_{^{111}\text{In, liver/lungs}})/(\mu_{^{57}\text{Co, liver/lungs}})}, \quad \text{Eq. 2}$$

where N_{pt} and $N_{\text{no pt}}$ are liver ROI counts in ^{57}Co transmission images with and without the patient, and $\mu^{57\text{Co, liver/lungs}}$ and $\mu^{111\text{In, liver/lungs}}$ are determined experimentally from the liver phantom studies described. For kidneys, spleen, and tumor dosimetry, ^{111}In photon attenuation was corrected using measured $\mu_{^{111}\text{In}}$ values determined from the 150- and 50-mL phantom studies. The depth of kidneys, spleen, and tumors from the body surface were measured from CT images.

Uptake of $^{90}\text{Y}/^{111}\text{In}$ in organs and tumors was expressed as the percentage of injected dose (%ID) at various imaging time points. The cumulated activity and biologic clearance half-life ($t_{b1/2}$) were determined by fitting the uptake data with a mono-exponential curve. If fit of a monoexponential curve was not possible, as uptake data continuously increased during the period of sequential imaging, cumulated activity was determined using the trapezoid method and a conservative estimation of the tail was used with a clearance rate of the physical half-life. For dosimetry purposes, the cumulated activity of ^{90}Y was determined from the biodistribution of ^{111}In and adjusted for the small difference in the physical half-life between ^{111}In and ^{90}Y .

Patient-Specific Radiation Dosimetry

Patient-specific radiation doses to organs and tumors were calculated based on the MIRD formalism (20):

$$D = \tilde{A} \sum \phi \Delta / m, \quad \text{Eq. 3}$$

where \tilde{A} is the cumulated activity determined by the image quantification; ϕ is the absorbed fraction for each energy deposition; Δ is the total equilibrium dose constant, mean energy emitted per nuclear transition, for each energy; and m is the patient-specific target mass. ^{90}Y is a pure, long-range β -emitter with an x_{90} (distance from the source within which 90% of the energy is absorbed) of 5.2 mm (21). The radiation absorbed fraction for each organ and tumor mass was interpolated using data of Siegel and Stabin (22), except for bone marrow.

Organ and tumor masses, except for bone marrow, were determined from CT images 1–2 wk before radioactivity administration. All patients had CT images of the chest, abdomen, and pelvis with a slice thickness of 5 mm. CT images were digitized using a high-resolution film scanner (Vidar System Co.) or imported directly through a DICOM (Digital Imaging and Communications in Medicine) network. Tissue volumes were determined using software developed in-house on the Interactive Data Language platform (Research Systems). Organ or tumor ROIs were drawn on each transverse slice. The area of each ROI was multiplied by the slice thickness to obtain the volume of interest in that slice. Total volume was then obtained by summing all volumes of interest (23).

Because patient-specific marrow dose from β -emissions in the blood does not require an explicit estimate of marrow mass, radiation dose was determined by (24):

$$D_{\text{RM}} = \Delta_{^{90}\text{Y}} \times \phi_{^{90}\text{Y}}(\text{RM} \leftarrow \text{RM}) \times \text{RMBLR} \times C_{\text{blood}}, \quad \text{Eq. 4}$$

where $\Delta_{^{90}\text{Y}} = 1.49\text{E}-13$ Gy·kg/Bq·s (25); $\phi_{^{90}\text{Y}}(\text{RM} \leftarrow \text{RM}) = 0.65$ (26); RMBLR (red marrow-to-blood concentration ratio) = 0.75 assuming a value between that of intact antibody and free radionuclides for the small molecular weight of DOTA-biotin/CC49-(scFv)₄SA; and C_{blood} is the concentration of cumulated radioactivity measured in the blood.

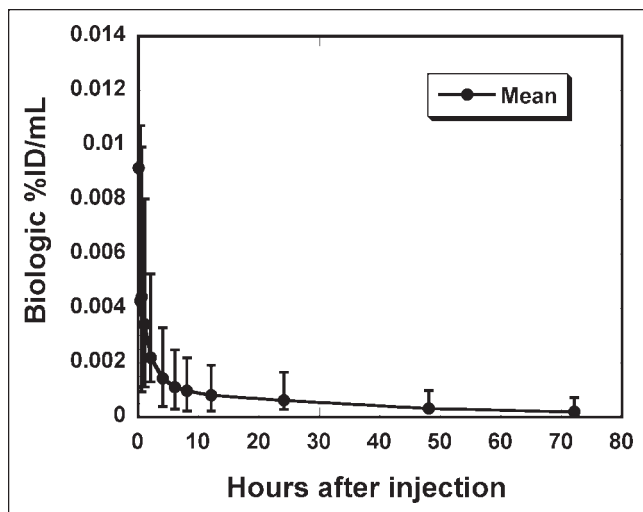


FIGURE 1. Mean serum (●) pharmacokinetic values (%ID/mL) after injection of ^{90}Y -DOTA-biotin. Error bars represent minimum and maximum values of 9 patients.

For organs that were not clearly visible, radiation doses were calculated using the remainder of the body:

$$D_{\text{RB}} = \bar{A}_{\text{RB}} \times \Delta_{90\text{Y}}/m_{\text{RB}}, \quad \text{Eq. 5}$$

where \bar{A}_{RB} or m_{RB} is the cumulated activity or the mass of the remainder of the body determined by subtraction of organ activities or masses from that of the total body, respectively.

For comparison, standard radiation dose estimates were also calculated using MIRD Pamphlet No. 11 (26) based on Reference Man's phantom data, which generate results similar to those using the MIRDOSE III program (27).

RESULTS

Quantification of $^{90}\text{Y}/^{111}\text{In}$ in Serum

With most elimination through the urine, <10% of the injected $^{90}\text{Y}/^{111}\text{In}$ -DOTA-biotin remained in the circulation after 8 h. The biphasic serum clearance curve of $^{90}\text{Y}/^{111}\text{In}$ -DOTA-biotin is illustrated in Figure 1. The concentration of ^{90}Y -DOTA-biotin in serum quickly dropped below 0.002

%ID/mL about 2 h after injection of ^{90}Y -DOTA-biotin. The range (minimum to maximum) of variation among 9 patients was modest (Table 2). The α -clearance phase, accounting for 90% of the dose, had a mean biologic half-life of 0.5 h, with a mean intercept of 0.0075 %ID/mL. The β -clearance phase had a mean biologic half-life of 18.3 h and a mean intercept of 0.0012 %ID/mL.

In patients 4–9, serum clearance between ^{111}In and ^{90}Y measurements was fairly close for each of these 6 patients (Fig. 2). The difference in mean weighted %ID/mL between ^{111}In and ^{90}Y was –2.8% for patient 4, 18.9% for patient 5, 21.4% for patient 6, –25.4% for patient 7, –3.0% for patient 8, and 13.2% for patient 9. The mean difference of absolute values in mean weighted %ID/mL was 14.1% (mean difference, 3.7%) between ^{111}In and ^{90}Y .

Quantitative Imaging

Phantom Studies. Transmission counts versus depth almost fit a straight line on a semilogarithmic plot for 50- and 150-mL ^{111}In sources (Fig. 3), with the linear regression correlation coefficient $R^2 > 0.99$. The linear attenuation coefficients ($\mu_{^{111}\text{In}}$) were determined to be 0.126 cm^{-1} for the 50-mL ^{111}In source and 0.122 cm^{-1} for the 150-mL ^{111}In source. Subsequently, the value of 0.126 cm^{-1} was used for attenuation correction of tumors ≤ 50 g. A value of 0.122 cm^{-1} was used for attenuation correction of kidney, spleen, and large tumors of ≥ 150 g.

Transmission fractions were determined for a liver phantom at various depths (Fig. 4). There was a small difference between the linear attenuation coefficient obtained from transmission of the ^{111}In in the liver phantom (0.113 cm^{-1}) and that obtained from the transmission scan using a ^{57}Co sheet source (0.119 cm^{-1}) (Fig. 3). Subsequently, the ACF for the following patient studies was determined by $(N_{\text{no pt}}/N_{\text{pt}})^{0.475}$ for liver quantification according to Equation 2.

Patient Studies. In addition to whole-body ROI counts, ROI counts were obtained for liver, spleen, kidneys, bladder, and tumors, as they were visualized above body

TABLE 2
Biphasic Clearance Parameters for Pharmacokinetics of ^{90}Y -DOTA-Biotin in Serum

Patient no.*	α -Phase intercept A1 (%ID/mL)	β -Phase intercept A2 (%ID/mL)	α -Phase (biologic) (h)	β -Phase (biologic) (h)
1	0.00915	0.00127	0.6	28.7
2	0.00908	0.00128	0.6	28.8
3	0.00697	0.00098	0.6	17.8
4	0.00875	0.00138	0.6	13.6
5	0.00321	0.00131	0.5	9.6
6	0.00859	0.00119	0.4	11.1
7	0.00722	0.00173	0.4	14.7
8	0.00715	0.00086	0.4	13.1
9	0.00735	0.00080	0.4	27.0

* ^{90}Y data for patients 1–3 were derived from ^{111}In . ^{90}Y data for patients 4–9 were measured directly.

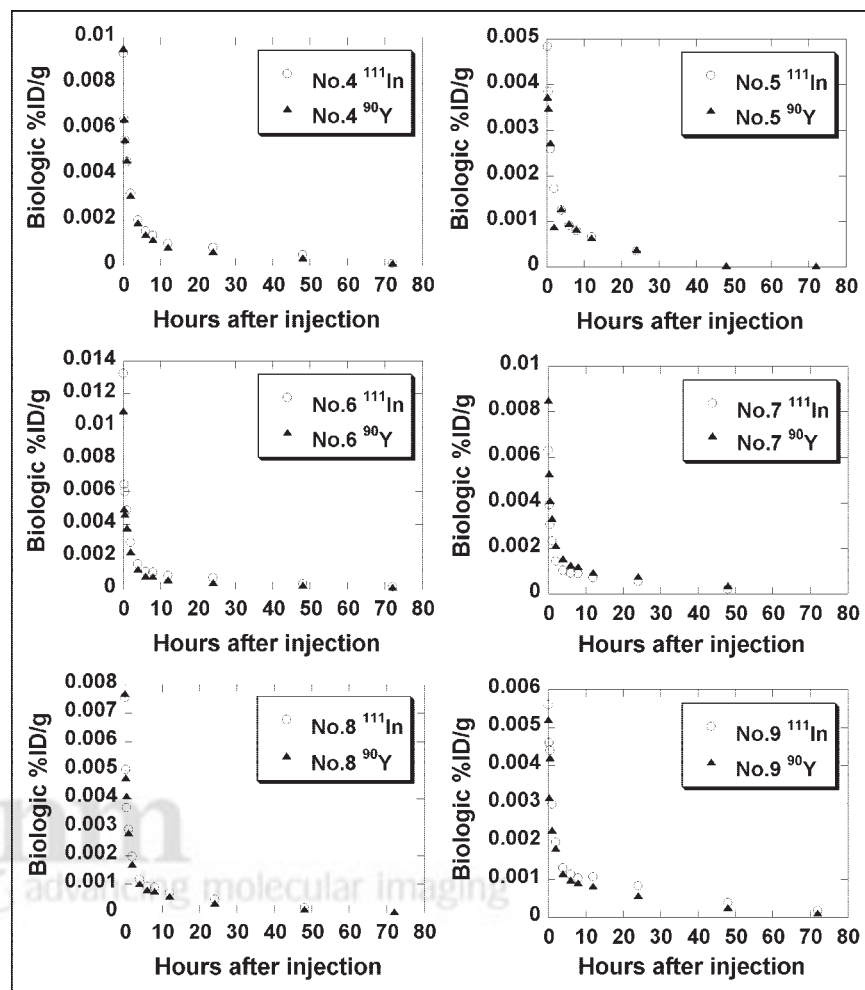


FIGURE 2. Serum concentration (%ID/mL) of ^{90}Y -DOTA-biotin and ^{111}In -DOTA-biotin measured in patients 4–9. Serum clearance between ^{90}Y and ^{111}In measurements was fairly close.

background (Fig. 5). Except for the whole body, tissue uptake in %ID/g was determined using patient-specific tissue masses measured from CT images. The mean patient body weight was 86.5 kg, with a range of 63.6–113.0 kg. The mean organ masses were 2,616 g (range, 1,263–3,855 g) for liver, 380 g (range, 95–1,009 g) for spleen, 437 g (range, 307–598 g) for kidneys, and 2,044 g (range, 1,560–2,884 g; $n = 3$, assuming lung density of 0.3 g/mL (28)) for lungs (Table 3). Although tumors were visualized in each patient, 13 tumors in 7 of 9 patients met the criteria for image quantification as described and were quantified. The mean tumor mass was 38.3 g (range, 1.1–200.0 g). The mean depth (from the center of the organ to the body surface) was 10.6 cm for kidneys and 8.3 cm for the spleen. Correspondingly, the mean attenuation correction factor was 3.64 for kidneys and 2.75 for spleen using the above measured $\mu_{^{111}\text{In}}$.

The peak uptake in normal organs usually occurred at the initial imaging time point. The peak occurred at a later imaging time in 5 of 13 tumors (Fig. 6) and in liver for 2 of the 9 patients. In general, the $t_{b1/2}$ of kidneys was shorter than that of liver and spleen. The mean $t_{b1/2}$ was 48 h for the whole body, 207 h for normal liver, 97 h for

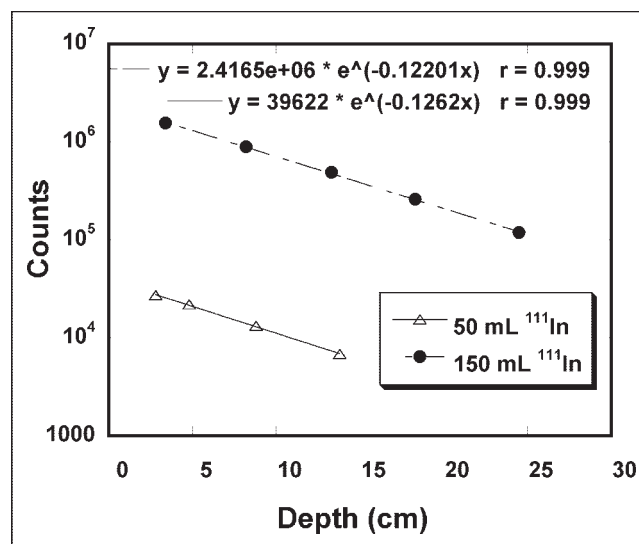


FIGURE 3. Transmission counts vs. source depth. ^{111}In sources of 50 and 150 mL were used to simulate tumor and kidney/spleen, respectively. Source depth was defined as solid water thickness added to distance of source center from source surface. Caret (^) is exponentiation operator.

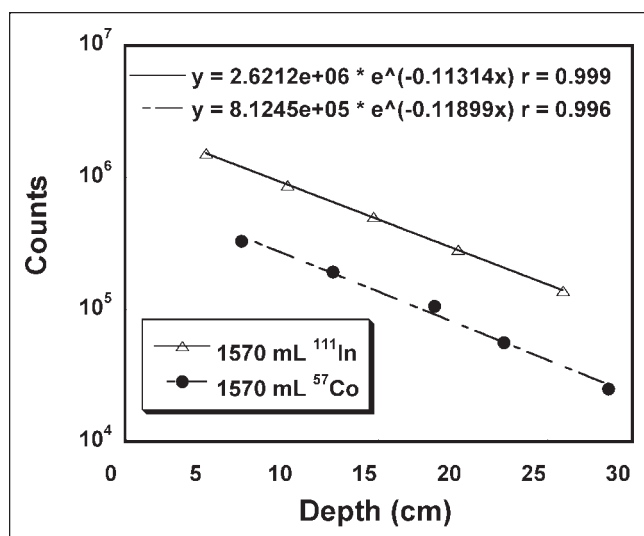


FIGURE 4. Transmission counts vs. source depth. ^{111}In source of 1,570 mL was used to simulate liver (Δ). Liver phantom transmission counts were also determined using ^{57}Co sheet source (\bullet). Source depth was defined as solid water thickness (2–24 cm) added to distance of source center from source surface. Caret (^) is exponentiation operator.

spleen, 77 h for kidney, 65 h for lung, and 133 h for tumors. Tumors had the highest peak uptake per gram of tissue mass (%ID/g) among all tissues (Table 4). The mean peak %ID/g was 0.032 for tumor, 0.0028 for normal liver, 0.0032 for spleen, 0.012 for kidney, and 0.0005 for lung.

Patient-Specific Dosimetry

Organ doses based on MIRD Reference Man's phantom mass versus patient-specific masses are compared in Table 5. The mean patient-specific body dose was 0.53 cGy/37 MBq. The mean patient-specific organ doses include 3.75 cGy/37 MBq for normal liver, 2.32 cGy/37 MBq for spleen, 7.02 cGy/37 MBq for kidneys, 0.30

cGy/37 MBq for lungs, 0.22 cGy/37 MBq for marrow, and 28.9 cGy/37 MBq for tumors. The tumor-to-normal tissue dose ratio was 54.5 for the whole body, 7.7 for normal liver, 12.5 for spleen, 4.1 for kidney, 96.3 for lung, and 131.4 for marrow.

There was substantial variation in organ dose from patient to patient. The ratios of the highest dose to the lowest dose among 9 patients were 10.9 for normal liver, 7.7 for spleen, 3.3 for kidneys, 4.9 for lungs, and 2.8 for marrow. Considerable differences in organ doses were noted dependent on use of MIRD Reference Man's phantom data versus patient-specific masses. The deviation of actual dose from MIRD Reference Man's model was as much as 11% underestimation or 59% overestimation for the whole body, 30% underestimation or 113% overestimation for normal liver, 47% underestimation or 454% overestimation for spleen, 92% overestimation for kidney, and 190% overestimation for lung.

DISCUSSION

CC49 is a second-generation murine antibody with anti-TAG-72 (tumor-associated antigen) reactivity to gastric, pancreatic, and colon adenocarcinomas (29). A single intravenous administration of ^{131}I -CC49 has been used in phase I and phase II clinical trials at multiple institutions for metastatic GI cancers (5–7,30). With 1.11–3.33 GBq/m² (30–90 mCi/m²), no objective tumor responses were observed and limited normal organ and tumor dosimetry was reported. In a high-dose study (7), patients received a single dose of 1.85–11.1 GBq/m² (50–300 mCi/m²) ^{131}I -CC49 after collection and cryopreservation of hematopoietic stem cells adequate for 2 autologous transplants. No objective responses were observed with a mean tumor-to-marrow ratio of 4.0 (range, 2.5–6.1) in the 5 patients analyzed. Although extra-hematopoietic dose-limiting toxicity was neither observed nor predicted, suboptimal tumor uptake (%ID/g, 0.0002–

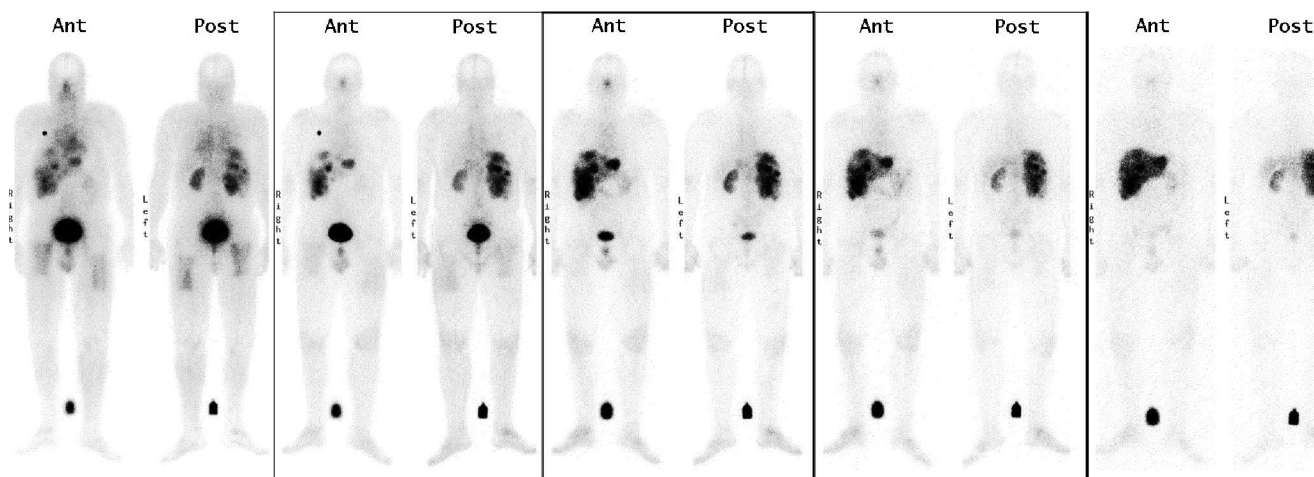


FIGURE 5. Whole-body images of ^{111}In -DOTA-biotin immediately, 3 h, 1 d, 2 d, and 4 d after injection. Liver, spleen, kidneys, bladder, and tumors in liver were visualized above body background. Ant = anterior; Post = posterior.

TABLE 3
Patient Body Weight and Organ/Tumor Masses Determined by CT Images

Patient no.	Body mass (g)	Liver mass (g)	Spleen		Kidneys		Lungs mass* (g)	Tumor	
			Mass (g)	Depth (cm)	Mass (g)	Depth (cm)		Mass (g)	Depth (cm)
1	84.5	1,659	95	7.8	374	11.9	2,884	32.5	7.9
2	113	2,304	215	12.7	598	13.6		14.3, 14	8.0, 13.7
3	75	2,330	311	8.1	371	10.4		3.5, 1.1	3.1, 8.2
4	63.6	1,263	201	8.8	307	8.5	1,560		
5	85.9	3,855	380	6.1	570	10.3	1,688		
6	70.9	1,732	152	6	368	8.1		26, 31	5.9, 9.2
7	109	3,213	1,009	11.6	414	13.9		57.5	6.8
8	83.2	3,378	782	6	439	8.9		200, 45.3, 26	†, 8.5, 6.5
9	93.6	3,811	278	7.3	495	4.7		32.1, 14.4	5.1, 4.7

*Lungs were not visualized above body background. Lungs of 3 patients were randomly selected to illustrate that lung doses were \leq body doses.

†Transmission scan was used for attenuation correction of this 200-g tumor.

0.0021) suggested that further escalation of ^{131}I -CC49 would not be useful (7).

In a subsequent high-dose study using long-range β -radiation, patients received a single dose of 11.1–18.5 MBq/kg (0.3–0.5 mCi/kg) ^{90}Y -CC49 after collection and cryopreservation of hematopoietic stem cells (9). Although 2 of 12 patients had stable disease durable for 2 and 4 mo, no objective responses were observed. The patient-specific dose for liver, spleen, and tumor based on SPECT plus the marrow dose based on activity in the blood were reported (Table 6) (9,30). Because our current study and the studies of Tempero et al. (9) and Lechner et al. (30) used the same radionuclides, $^{90}\text{Y}/^{111}\text{In}$, the difference in tissue dosimetry should be mainly due to the difference in tissue distribution of intact antibody CC49 and pretargeted CC49-(scFv) $_4$ SA. The radiation dose per

injected activity to each reported normal organ (liver, spleen, and marrow) was smaller using pretargeted CC49-(scFv) $_4$ SA compared with that of intact CC49 (Table 6), whereas the tumor-to-normal organ dose ratios were >8 -fold greater for liver and marrow.

A few previous clinical trials using the pretargeted system have been performed. ^{90}Y -DOTA-biotin after NR-LU-10-SA has been conducted for patients with metastatic colon cancer (11). Unfortunately, the results of this phase II trial were not encouraging due to a high incidence of GI toxicity resulting from cross-reactivity of the NR-LU-10 with the bowel epithelium. The estimated mean radiation dose to the small intestine could be as high as 66.5 cGy/37 MBq (or rad/mCi) (11). Consequently, the advantage of pretargeting was not realized using NR-LU-10 antibody. Imaging (Fig. 5) and dosimetry (Table 5) results of the current study are consistent with prior clinical trials of murine CC49 antibody, demonstrating no observable cross-reactivity with normal tissues. The proof of principle of the potential advantages of pretargeting has been demonstrated in lymphoma patients, where tumor-to-normal tissue ratios for liver, spleen, and marrow have been >50 (14,16).

Because of the relatively small molecular size of the DOTA-biotin and rapid urinary excretion of unbound ^{90}Y -DOTA-biotin, the kidney could be the potential dose-limiting organ for pretargeting with CC49-(scFv) $_4$. Though there was no direct report on kidney dosimetry for colon cancer trials using CC49, a similar trial using ^{131}I -CC49 and α -interferon for prostate cancer reported a kidney dose of 4.9 cGy/37 MBq (4.9 rad/mCi) (31). The mean tumor-to-kidney dose ratio was 3.9 for ^{131}I -CC49 compared with a mean dose ratio of 4.1 for pretargeted CC49-(scFv) $_4$ of the current study. Projecting for a kidney dose at tolerance level ($\text{TD}_{5/5}$ [the probability of 5% complication within 5 y]) of 2,300 cGy, as used for fractionated external-beam radiation (32), the mean radi-

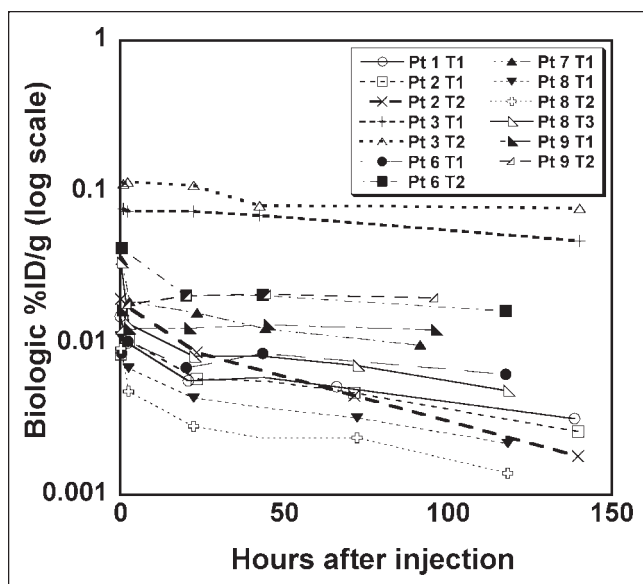


FIGURE 6. Tumor %ID/g vs. time for 13 tumors in 7 patients.

TABLE 4
 $t_{b1/2}$ and Peak Tissue Uptake as Percentage Injected Dose per Gram (%ID/g)

Patient no.	Body $t_{b1/2}$ (h)	Liver		Spleen		Kidneys		Lung*		Tumor	
		$t_{b1/2}$ (h)	Peak %ID/g	$t_{b1/2}$ (h)	Peak %ID/g	$t_{b1/2}$ (h)	Peak %ID/g	$t_{b1/2}$ (h)	Peak %ID/g	$t_{b1/2}$ (h)	Peak %ID/g
1	62	222	0.0028	144	0.0048	133	0.012	70	0.00033	74	0.015
2	49	81	0.0014	75	0.0037	71	0.010			77, 41	0.011, 0.020
3	61	541	0.0042	171	0.0047	40	0.012			NA, 285	0.077, 0.117
4	36	122	0.0012	182	0.0020	84	0.006	22	0.00071		
5	62	1,560	0.0033	NA	0.0016	39	0.016	102	0.00050		
6	44	296	0.0041 [†]	111	0.0042	77	0.018			218, 92	0.010, 0.043
7	35	106	0.0033 [†]	67	0.0038	81	0.016			62	0.035
8	40	83	0.0021 [†]	110	0.0013	74	0.012			68, 60, 63	0.011, 0.009, 0.017
9	41	NA	0.0032 [†]	172	0.0025	91	0.004			436, NA	0.017, 0.021

*Lungs were not visualized above body background. Lungs of 3 patients were randomly selected to illustrate that lung doses were ≤ body doses.

[†]Normal liver excluding tumors.

NA = clearance half-life not available because of increased uptake within 144-h observation period.

ation dose to tumor from the pretargeting scheme of CC49-(scFv)₄SA followed by ⁹⁰Y- DOTA-biotin would be 9,460 cGy. This mean dose is much higher than reported—180–3,000 cGy from ⁹⁰Y-CC49 (9) or 630–3,300 cGy from ¹³¹I-CC49 (7)—and is expected to be cytotoxic to GI adenocarcinomas.

MIRD dosimetry based on a patient population-averaged Reference Man's phantom provides a convenient method for organ dose estimates when exact organ masses are not available or are difficult to obtain. However, organ dose can be substantially under- or overestimated because of the large variation in organ size. In the current study, we noted that organ doses were more likely to be overestimated using Reference Man's mass. This is

likely due to the tendency that body weight and organ masses in the current population are larger than that of Reference Man measured decades ago (33).

The experimental methods described here to determine $\mu_{^{111}\text{In}}$ and $\text{ACF}_{^{111}\text{In}}$ using the ¹¹¹In phantom and ⁵⁷Co flood source can be applied to determine μ and ACF for other radionuclides. However, the numeric values of $\mu_{^{111}\text{In}}$ and $\text{ACF}_{^{111}\text{In}}$ reported here cannot be simply applied to γ -cameras of different specifications without confirmation. Our camera had 3/4-in. NaI(Tl) crystals compared with 3/8-in. crystals commonly used in most clinical settings.

There are uncertainties in marrow dose estimation using the standard blood method for ¹¹¹In/⁹⁰Y-labeled phar-

TABLE 5
Radiation Dose per Injected Activity (cGy/37 MBq) Based on MIRD Reference Man's Mass and Patient-Specific Organ Mass

Patient no.	cGy/37 MBq (or rad/mCi)											
	Body		Liver		Spleen		Kidneys		Lungs*		Marrow, Sp	Tumor, Sp
	Ref	Sp	Ref	Sp	Ref	Sp	Ref	Sp	Ref	Sp		
1	0.65	0.55	1.84	2.00	1.34	2.56	10.05	8.35	0.26	0.09	0.34	8.9
2	0.51	0.32	0.80	0.63	1.78	1.50	9.41	4.90			0.27	7.9, 10.4
3	0.82	0.78	8.88	6.89	7.67	4.46	12.03	10.08			0.30	94.3, 121.6
4	0.50	0.56	3.11	4.46	1.90	1.71	5.93	6.01	0.59	0.37	0.21	
5	0.84	0.69	9.87	4.63	5.82	2.77	11.97	6.53	0.74	0.44	0.13	
6	0.64	0.64	5.78 [†]	6.03 [†]	2.41	2.87	8.38	7.08			0.15	11.7, 34.2
7	0.57	0.37	4.74 [†]	2.67 [†]	12.10	2.17	14.98	11.25			0.24	20.0
8	0.45	0.39	2.20 [†]	1.18 [†]	2.49	0.58	7.94	5.62			0.12	6.4, 4.2, 6.6
9	0.59	0.45	11.11 [†]	5.27 [†]	3.47	2.25	5.36	3.36			0.21	21.0, 33.8

*Lungs were not visualized above body background. Lungs of 3 patients were randomly selected to illustrate that lung doses were ≤ body doses.

[†]Normal liver excluding tumors.

Ref = MIRD Reference Man's mass; Sp = patient-specific organ mass.

TABLE 6

Comparison of Mean (and Range) of Patient-Specific Organ and Tumor Doses for Directly Labeled Intact $^{90}\text{Y}/^{111}\text{In}$ -CC49 Antibody and Pretargeted CC49 Fusion Protein Followed by ^{90}Y -DOTA-Biotin

Organ or tumor	Radiation dose (cGy/37 MBq)		Tumor-to-normal organ dose ratio	
	^{90}Y -CC49*	Pretargeted ^{90}Y -DOTA-biotin	^{90}Y -CC49*	Pretargeted ^{90}Y -DOTA-biotin
Liver	37.4 (17.0–80.9)	3.75 (0.63–6.89)	0.9 (0.3–1.5)	8.0 (1.9–17.6)
Spleen	30.1 (12.0–62.5)	2.32 (0.58–4.46)	1.2 (0.5–3.0)	10.5 (3.5–27.3)
Marrow	2.5 (1.6–4.0)	0.22 (0.12–0.34)	15.2 (3.6–42.1)	117.4 (25.8–399.1)
Tumor	34.5 (7.0–80.9)	28.9 (4.18–121.6)		

*Data from Leichner et al. (30).

maceuticals (34) since the small portion of free ^{90}Y -chelator or ^{90}Y could have a different distribution compared with that of the small portion of free ^{111}In -chelator or ^{111}In (35). The blood method assumes no specific uptake of $^{111}\text{In}/^{90}\text{Y}$ in marrow. This assumption becomes invalid if marrow has active uptake or free $^{111}\text{In}/^{90}\text{Y}$ or $^{111}\text{In}/^{90}\text{Y}$ -cheletor is recycled into the marrow space/trabecular bone surface after radiopharmaceuticals are metabolized. In the current study, CC49 fusion protein does not bind to marrow. The amount of free $^{111}\text{In}/^{90}\text{Y}$ or $^{111}\text{In}/^{90}\text{Y}$ -chelator recycled into the marrow space/trabecular bone surface may not be significant because marrow was not visualized above body background in our patient images. In other $^{111}\text{In}/^{90}\text{Y}$ -antibody studies, ^{111}In was visualized in the marrow even when the antibodies were nonmarrow binding (34). In pretargeted NR-Lu-10/SA, where ^{111}In was not visible in marrow, the blood method worked well for predicting ^{90}Y -induced toxicity ($r = 0.77$) (10). Extrapolation of ^{90}Y concentration in serum from ^{111}In introduces another uncertainty. However, in the current study, serum clearance between ^{111}In and ^{90}Y measurements was fairly close for each of these 6 patients (Fig. 2). The mean difference of absolute values in mean weighted %ID was 14.1% between ^{111}In and ^{90}Y in 6 patients.

CONCLUSION

The dosimetry results of the current study demonstrate substantially improved tumor-to-normal tissue dose ratios compared with that of previously reported RIT trials for metastatic GI cancer.

ACKNOWLEDGMENTS

This work was partly supported by NeoRx Corp. and grants P50 CA89019-03 and MO1 RR 00032 from the National Cancer Institute.

REFERENCES

- DeNardo SJ, DeNardo GL, O'Grady LF, et al. Treatment of B cell malignancies with ^{131}I Lym-1 monoclonal antibodies. *Int J Cancer*. 1988;3(suppl):96–101.
- Press OW, Eary JF, Appelbaum FR, et al. Radiolabeled-antibody therapy of B-cell lymphoma with autologous bone marrow support. *N Engl J Med*. 1993;329:1219–1224.
- Kaminski MS, Zasadny KR, Francis IR, et al. Radioimmunotherapy of B-cell lymphoma with ^{131}I anti-B1 (anti-CD20) antibody. *N Engl J Med*. 1993;329:459–465.
- Wiseman GA, White CA, Stabin M, et al. Phase I/II ^{90}Y -Zevalin (yttrium-90 ibritumomab tiuxetan, IDEC-Y2B8) radioimmunotherapy dosimetry results in relapsed or refractory non-Hodgkin's lymphoma. *Eur J Nucl Med*. 2000;27:766–777.
- Divgi CR, Scott AM, Dantis L, et al. Phase I radioimmunotherapy trial with iodine-131-CC49 in metastatic colon carcinoma. *J Nucl Med*. 1995;36:586–592.
- Murray JL, Macey DJ, Grant EJ, et al. Enhanced TAG-72 expression and tumor uptake of radiolabeled monoclonal antibody CC49 in metastatic breast cancer patients following alpha-interferon treatment. *Cancer Res*. 1995;55(suppl):5925–5928.
- Tempero M, Leichner P, Dalrymple G, et al. High-dose therapy with iodine-131-labeled monoclonal antibody CC49 in patients with gastrointestinal cancers: a phase I trial. *J Clin Oncol*. 1997;15:1518–1528.
- Meredith RF, Khazaeli MB, Plott WE, et al. Phase II study of dual ^{131}I -labeled monoclonal antibody therapy with interferon in patients with metastatic colorectal cancer. *Clin Cancer Res*. 1996;2:1811–1818.
- Tempero M, Leichner P, Baranowska-Kortylewicz J, et al. High-dose therapy with ^{90}Y -labeled monoclonal antibody CC49: a phase I trial. *Clin Cancer Res*. 2000;6:3095–3102.
- Breitz HB, Fisher DR, Goris ML, et al. Radiation absorbed dose estimation for ^{90}Y -DOTA-biotin with pretargeted NR-LU-10/streptavidin. *Cancer Biother Radiopharm*. 1999;14:381–395.
- Knox SJ, Goris ML, Tempero M, et al. Phase II trial of yttrium-90-DOTA-biotin pretargeted by NR-LU-10 antibody/streptavidin in patients with metastatic colon cancer. *Clin Cancer Res*. 2000;6:406–414.
- Weiden PL, Breitz HB, Press O, et al. Pretargeted radioimmunotherapy (PRIT) for treatment of non-Hodgkin's lymphoma (NHL): initial phase I/II study results. *Cancer Biother Radiopharm*. 2000;15:15–29.
- Breitz HB, Weiden PL, Beaumier PL, et al. Clinical optimization of pretargeted radioimmunotherapy with antibody-streptavidin conjugate and ^{90}Y -DOTA-biotin. *J Nucl Med*. 2000;41:131–140.
- Weiden PL, Breitz HB. Pretargeted radioimmunotherapy (PRIT) for treatment of non-Hodgkin's lymphoma (NHL). *Crit Rev Oncol Hematol*. 2001;40:37–51.
- Axworthy DB, Reno JM, Hylarides MD, et al. Cure of human carcinoma xenografts by a single dose of pretargeted yttrium-90 with negligible toxicity. *Proc Natl Acad Sci USA*. 2000;97:1802–1807.
- Forero A, Weiden PL, Vose JM, et al. Phase I trial of a novel anti-CD20 fusion protein in pretargeted radioimmunotherapy for B-cell non-Hodgkin's lymphoma. *Blood*. 2004;104:227–236.
- Thomas SR, Maxon HR, Kereiakes JG. In vivo quantitation of lesion radioactivity using external counting methods. *Med Phys*. 1976;3:253–255.
- Shen S, DeNardo GL, DeNardo SJ. Quantitative bremsstrahlung imaging of yttrium-90 using a Wiener filter. *Med Phys*. 1994;21:1409–1417.
- DeNardo GL, Shen S, DeNardo SJ, et al. Quantification of iodine-131 in tumors using a threshold based on image contrast. *Eur J Nucl Med*. 1998;25:497–502.
- Loevinger R, Bermam M. *A Revised Schema for Calculating the Absorbed Dose from Biologically Distributed Radionuclides*. MIRD Pamphlet No. 1. New York, NY: Society of Nuclear Medicine; 1976.
- Berger MJ. Distribution of absorbed dose around point sources of electrons and

- beta particles in water and other media: MIRD Pamphlet No. 7. *J Nucl Med.* 1971;5(suppl):5–23.
22. Siegel JA, Stabin MG. Absorbed fractions for electrons and beta particles in spheres of various sizes. *J Nucl Med.* 1994;35:152–156.
 23. Shen S, DeNardo GL, O'Donnell RT, et al. Impact of splenomegaly on therapeutic response and I-131-LYM-1 dosimetry in patients with B-lymphocytic malignancies. *Cancer.* 1997;80:2553–2557.
 24. Shen S, DeNardo GL, Sgouros G, et al. Practical determination of patient-specific marrow dose using radioactivity concentration in blood and body. *J Nucl Med.* 1999;40:2102–2106.
 25. Dillman L, Von der Lage F. *Radionuclide Decay Schemes and Nuclear Parameters for Use in Radiation-Dose Estimation.* MIRD Pamphlet No. 10. New York, NY: Society of Nuclear Medicine; 1975.
 26. Snyder WS, Ford MR, Warner GG, Watson SB. 'S', *Absorbed Dose per Unit Cumulated Activity for Selected Radionuclides and Organs.* MIRD Pamphlet No. 11. New York, NY: Society of Nuclear Medicine; 1975.
 27. Stabin MG. MIRDose: personal computer software for internal dose assessment in nuclear medicine. *J Nucl Med.* 1996;37:538–546.
 28. Snyder WS, Fisher HL Jr, Ford MR, Warner GG. Estimates of absorbed fractions for monoenergetic photon sources uniformly distributed in various organs of a heterogeneous phantom. *J Nucl Med.* 1969;3(suppl):7–52.
 29. Molinolo A, Simpson JF, Thor A, Schlom J. Enhanced tumor binding using immuno-histochemical analyses by second generation anti-tumor-associated glycoprotein 72 monoclonal antibodies versus monoclonal antibody B72.3 in human tissue. *Cancer Res.* 1990;50:1291–1298.
 30. Lechner PK, Akabani G, Colcher D, et al. Patient-specific dosimetry of indium-111- and yttrium-90-labeled monoclonal antibody CC49. *J Nucl Med.* 1997;38:512–516.
 31. Meredith R, Shen S, Macey D, et al. Comparison of biodistribution, dosimetry, and outcome from clinical trials of radionuclide-CC49 antibody therapy. *Cancer Biother Radiopharm.* 2003;18:393–404.
 32. Emami B, Lyman J, Brown A, et al. Tolerance of normal tissue to therapeutic irradiation. *Int J Radiat Oncol Biol Phys.* 1991;21:109–122.
 33. Huh C, Bolch WE. A review of US anthropometric reference data (1971–2000) with comparisons to both stylized and tomographic anatomic models. *Phys Med Biol.* 2003;48:3411–3429.
 34. Shen S, Meredith RF, Duan J, et al. Improved prediction of myelotoxicity using a patient-specific imaging dose estimate for non-marrow-targeting ⁹⁰Y-antibody therapy. *J Nucl Med.* 2002;43:1245–1253.
 35. Lovqvist A, Humm JL, Sheikh A, et al. PET imaging of ⁸⁶Y-labeled anti-Lewis Y monoclonal antibodies in a nude mouse model: comparison between ⁸⁶Y and ¹¹¹In radiolabels. *J Nucl Med.* 2001;42:1281–1287.

